Article

Magneto-optics in a van der Waals magnet tuned by self-hybridized polaritons

https://doi.org/10.1038/s41586-023-06275-2

Received: 18 January 2023

Accepted: 31 May 2023

Published online: 16 August 2023

Check for updates

Florian Dirnberger[1,11]✉, Jiamin Quan[2,3,4,11], Rezlind Bushati[1,2], Geoffrey M. Diederich[5,6], Matthias Florian[7], Julian Klein[8], Kseniia Mosina[9], Zdenek Sofer[9], Xiaodong Xu[6], Akashdeep Kamra[10], Francisco J. García-Vidal[10], Andrea Alù[2,3,4]✉ & Vinod M. Menon[1,2]✉

Controlling quantum materials with light is of fundamental and technological importance. By utilizing the strong coupling of light and matter in optical cavities[1–3], recent studies were able to modify some of their most defining features[4–6]. Here we study the magneto-optical properties of a van der Waals magnet that supports strong coupling of photons and excitons even in the absence of external cavity mirrors. In this material—the layered magnetic semiconductor CrSBr—emergent light–matter hybrids called polaritons are shown to substantially increase the spectral bandwidth of correlations between the magnetic, electronic and optical properties, enabling largely tunable optical responses to applied magnetic fields and magnons. Our results highlight the importance of exciton–photon self-hybridization in van der Waals magnets and motivate novel directions for the manipulation of quantum material properties by strong light–matter coupling.

Magnetic responses of optical excitations in solids are the key to efficiently interfacing magnetism and light, but materials supporting strong responses are rare. It thus attracted considerable interest when studies recently demonstrated the exceptional magneto-optical properties of magnetic van der Waals (vdW) crystals[7–11]. In these layered materials, spin-related phenomena, like the magneto-optical Kerr effect[12,13], linear magnetic dichroism[14] and inherently polarized light emission[7,15], are often significantly enhanced in the spectral region of magnetic excitons—an intriguing type of optical excitation formed by spin-polarized electronic states in magnets. As a natural link between photons and spins, these magnetic excitons offer a unique opportunity to investigate the impact of strong exciton–photon coupling on the magneto-optical properties of layered magnetic systems.

An archetypal vdW material to leverage the effects of strong coupling is the antiferromagnetic (AFM) semiconductor CrSBr. Its optical spectrum supports pronounced excitonic signatures in the near-infrared region, and moderately strong magnetic fields are sufficient to switch the equilibrium AFM order into a ferromagnetic (FM) configuration (Fig. 1a) below the Néel temperature $T_N = 132$ K (ref. 10), revealing an intimate relation between the electronic and magnetic structures. Opposed to magneto-optic effects that modulate the polarization of light, this relation directly alters the optical spectrum by modifying the exciton energy[10].

Here, we demonstrate the impact of strong light–matter coupling on the optical and magneto-optical properties of the vdW magnet CrSBr. Hybridization of magnetic excitons and photons is shown to fully determine the optical response of mesoscopic crystals to applied magnetic fields and magnons. We observe a substantial enhancement of the spectral bandwidth of magneto-optic correlations due to the formation of tunable polaritons in crystals with and without external cavity mirrors. The excellent agreement between theoretical models and experimental observations highlights the virtually untapped potential of hybrid exciton–photon systems for magneto-optics.

Strong light–matter coupling in CrSBr

Before discussing magneto-optic phenomena, we address the confinement of photons and their strong coupling with excitons in CrSBr crystals of mesoscopic size (that is, for flake thicknesses varying from about 10 to 1,000 nm). Figure 1a depicts the two experimental configurations we use to confine optical modes. One traps photons inside bare crystals due to the large dielectric mismatch at the interfaces to the environment, leading to pronounced self-hybridization effects[16], while the other achieves larger photon confinement by adding highly reflective mirrors to the top and bottom surfaces. In both cases, we observe a strongly thickness-dependent series of optical states in the low-temperature optical reflectance, in stark contrast to the single-exciton resonance at approximately 1.34 eV reported for bilayer samples[10]. We are able to simulate the experimental reflectance signatures of different samples with and without external mirrors by modelling the dielectric function of CrSBr with just a single strong oscillator to account for the main excitonic transition (Fig. 1b and Supplementary Figs. 2–4). Figure 1c shows the simulated reflectance as a function of

[1]Department of Physics, City College of New York, New York, NY, USA. [2]Department of Physics, The Graduate Center, City University of New York, New York, NY, USA. [3]Photonics Initiative, CUNY Advanced Science Research Center, New York, NY, USA. [4]Department of Electrical Engineering, City College of the City University of New York, New York, NY, USA. [5]Intelligence Community Postdoctoral Research Fellowship Program, University of Washington, Seattle, WA, USA. [6]Department of Physics and Department of Materials Science and Engineering, University of Washington, Seattle, WA, USA. [7]Department of Electrical and Computer Engineering and Department of Physics, University of Michigan, Ann Arbor MI, USA. [8]Department of Materials Science and Engineering, Massachusetts Institute of Technology, Cambridge, MA, USA. [9]Department of Inorganic Chemistry, University of Chemistry and Technology Prague, Prague, Czech Republic. [10]Departamento de Física Teórica de la Materia Condensada and Condensed Matter Physics Center, Universidad Autónoma de Madrid, Madrid, Spain. [11]These authors contributed equally: Florian Dirnberger, Jiamin Quan. ✉e-mail: fdirnberger@ccny.cuny.edu; aalu@gc.cuny.edu; vmenon@ccny.cuny.edu

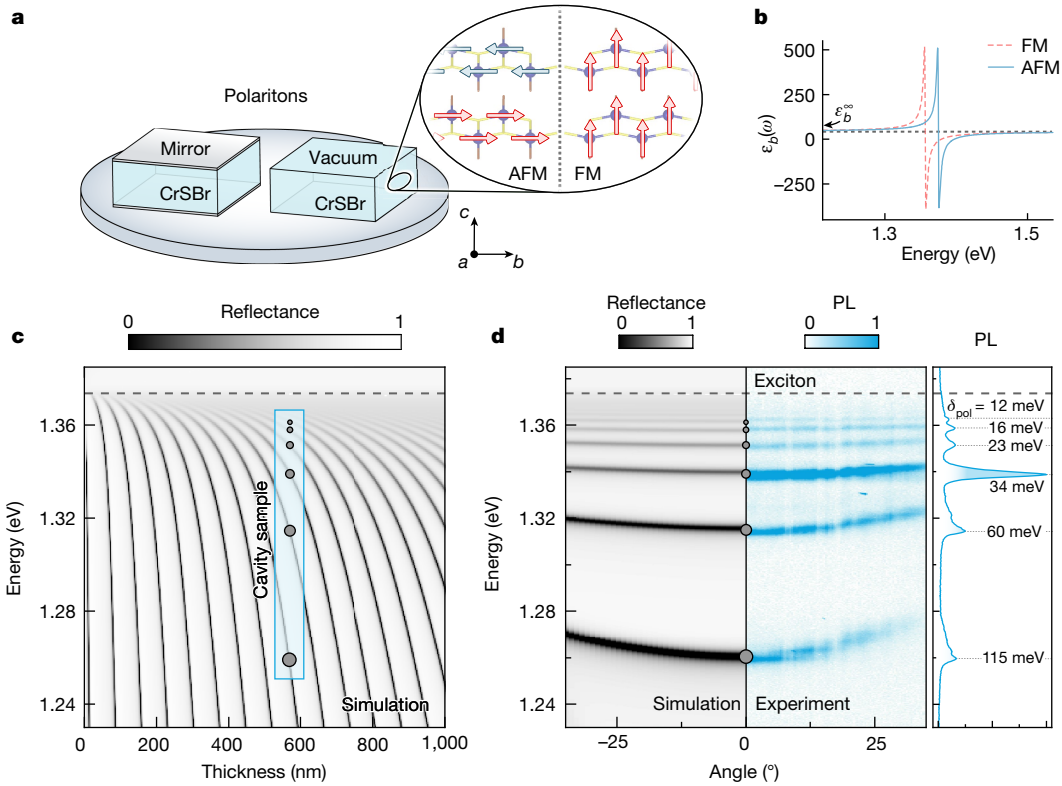

Fig. 1 | Exciton–photon coupling in CrSBr cavities. a, Schematic illustrating two experimental approaches to support exciton–polaritons in mesoscopic CrSBr: bare crystals on a SiO_2/Si substrate and crystals embedded between highly reflective bottom and top mirrors. The magnified view shows AFM and FM order ($B_{ext} \| c$). Magnetic axes are the crystal *b* (easy), *a* (intermediate) and *c* (hard) axes (compare Supplementary Fig. 1)[10]. **b**, Model dielectric functions of CrSBr derived in numerical calculations of optical reflectance spectra. **c**, Simulation of the reflectance of CrSBr crystals for different thicknesses. Six prominent polariton branches are observed in a 580-nm-thick sample with external cavity mirrors (grey circles). The exciton energy, $E_X = 1.374$ eV, determined from simulations is indicated by the dashed grey line. **d**, The right panel shows angle-resolved and angle-integrated PL emission of a nominally 580-nm-thick sample recorded at $T = 1.6$ K. The crystal was rotated by 45° with respect to the entrance slit of the spectrometer, and the PL was analysed with a polarizer along the *b* axis. The left panel shows the simulated reflectance map for conditions matching the experiment.

crystal thickness for samples enclosed by external mirrors (compare also polariton dispersion in bare crystals in Supplementary Fig. 2).

Our experiments and the theoretical models described in Supplementary Information Section 2 unambiguously identify the optical states in mesoscopic CrSBr crystals as the hybrid exciton–photon quasiparticles known as exciton–polaritons. Each state in the reflectance spectra corresponds to a specific branch of the polariton dispersion. Moreover, a comparison of our measurements with the model calculations demonstrates that the oscillator strength of excitons in CrSBr is amongst the largest known in solid-state systems, exceeding similar reports from gallium arsenide[17], transition-metal dichalcogenides[18] and hybrid perovskites[19,20]. With Rabi splitting energies reaching $\hbar\Omega_R \approx 0.24$ eV, light–matter interactions in CrSBr are so pronounced, they are ascribed to the ultrastrong coupling regime (Supplementary Information Section 2 and Supplementary Fig. 5), which provides an intuitive explanation for the dramatically different optical spectra of mesoscopic crystals compared with bilayer samples.

Due to the pronounced self-hybridization effects already present in bare crystals, the addition of highly reflective cavity mirrors does not significantly change the polariton dispersion, but both our experiments and our simulations show they can further enhance experimental polariton signatures (Supplementary Figs. 6 and 7). Figure 1d presents the angle-integrated and -resolved low-temperature photoluminescence (PL) emission of a 580-nm-thick flake with external cavity mirrors supporting six distinct polariton branches, all of which are in excellent agreement with the simulated and measured polariton reflectance spectra shown in Fig. 1d and Supplementary Fig. 8. A resonant state with small oscillator strength, potentially arising from defects[21], enhances the intensity of the polariton peak near 1.34 eV. More importantly, we note an increasing contribution from photons in polariton branches with large zero-angle detuning δ_{pol} from the exciton resonance. Their stronger curvature directly evidences the reduction of the effective polariton mass due to the mixing with photons (Supplementary Fig. 9). Overall, the different (average) exciton fractions *X* of each polariton branch in this sample are well suited to investigate the role of exciton–photon coupling in the magneto-optical responses of this material.

Tunable magneto-optic properties

Analogous to previous studies of the electric field response of polaritons[22,23], we investigate the effects of an external magnetic field B_{ext}. As described in Supplementary Information Section 3, a field along the magnetic hard axis causes the canting of spins, which alters the angle θ between the two sublattice magnetizations and results in a decrease of exciton energies, $\Delta E = \Delta_B \cos^2(\theta/2)$ (ref. 10). The PL emission of each branch in our 580-nm sample, therefore, shifts towards lower energies, along a bell-shaped curve, until saturation occurs at $B_{ext} = B_{sat}$ (Fig. 2a). We determine the maximum shift $\Delta_B(X)$ of polariton branches with different detuning δ_{pol} and exciton fraction *X* in several strongly coupled samples both with and without external mirrors and find that the magnetic field response of polaritons is strongly affected by hybridization. Figure 2b indicates a linear dependence of the magnetic shift on the exciton fraction *X*, which modifies the dispersion and the effective mass of polariton branches (Supplementary Fig. 9). While the largest energy shifts are obtained for exciton-like branches, the strongest reflectance responses occur for more photon-like polaritons due to a

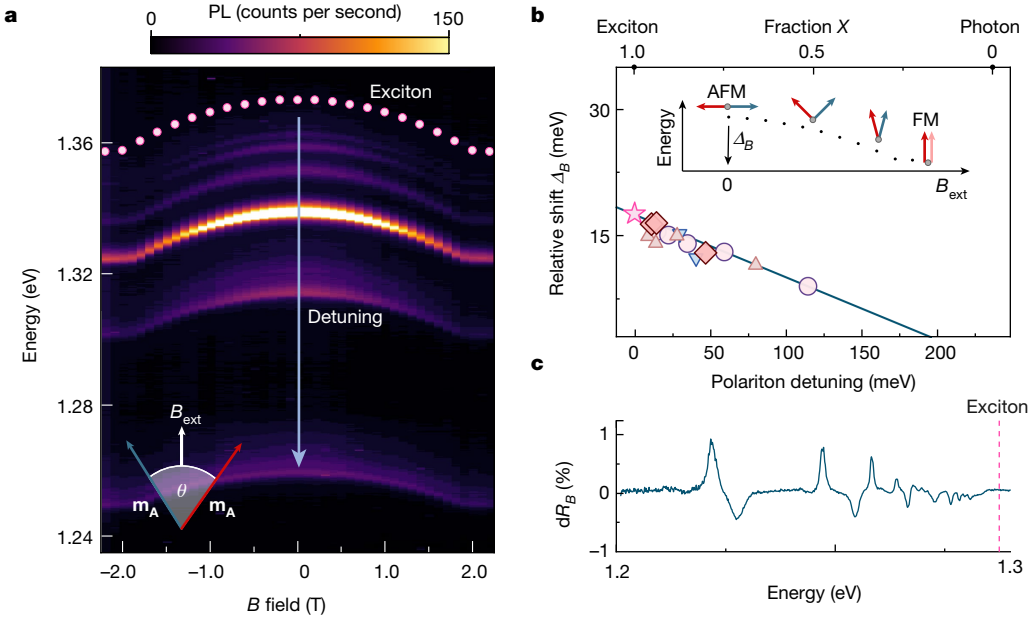

Fig. 2 | Magnetic field response of polaritons. a, Field-induced shift of the angle-integrated polariton PL emission. External field B_{ext} is applied along the *c* direction. Pink dots show the field dependence of excitons determined from numerical simulations, and blue and red arrows represent sublattice magnetizations $\mathbf{m_A}$ and $\mathbf{m_B}$. Data were collected at $T = 1.6$ K from the sample shown in Fig. 1d with a polarizer aligned along the *b* axis. **b**, Maximum field-induced shift Δ_B as a function of detuning δ_{pol}. Different symbols represent different samples with and without mirrors, and the same colours indicate polariton branches measured within each sample. The solid line shows the calculation $\Delta_B(X) = \Delta_B X$, where $\Delta_B = -17.5$ meV (star symbol) is extracted from our numerical simulations. The inset shows a schematic of field-induced spin canting and the resulting shift Δ_B. **c**, Field-induced changes in the reflectance spectrum dR_B of the sample shown in **a** ($B_{ext} = B_{sat}$).

decrease in absorption at lower energies (Fig. 2c). By transferring the correlation of the magnetic and electronic structures to polariton states deep inside the optical gap, strong coupling substantially increases the bandwidth of the magneto-optical response of CrSBr to an applied field. Hence, even at energies much below the exciton resonance, where bi- and few-layer samples are transparent, magnetic fields profoundly change the optical reflectance of mesoscopic CrSBr crystals by up to 90%.

Prominent magneto-optical effects can also be obtained by changing the internal magnetic order of CrSBr via magnons. Recent pump–probe

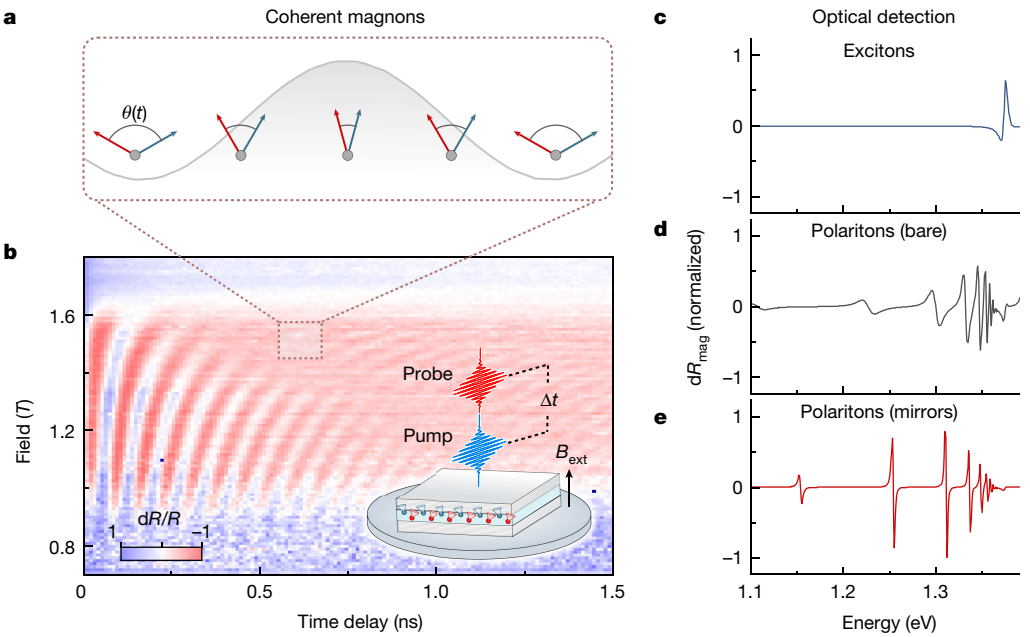

Fig. 3 | Polariton–magnon coupling and coherent magnon effects. **a**, Coherent magnon oscillations periodically modulate the angle $\theta(t)$ between the two sublattice magnetizations. **b**, Energy-integrated pump–probe measurement of the transient reflectance of two closely spaced exciton-like polariton branches ($X \approx 0.9$). The curve shows the normalized differential reflectance dR/R recorded at different fields B_{ext} applied along the *c* axis at $T = 50$ K. **c**–**e**, Calculations of the magnon-induced reflectance changes dR_{mag} based on the model described in Supplementary Information Section 4B for excitons in a bilayer (**c**) and polaritons in 580-nm-thick crystals without (**d**) and with external mirrors (**e**). Data are normalized to the maximum in **e**.

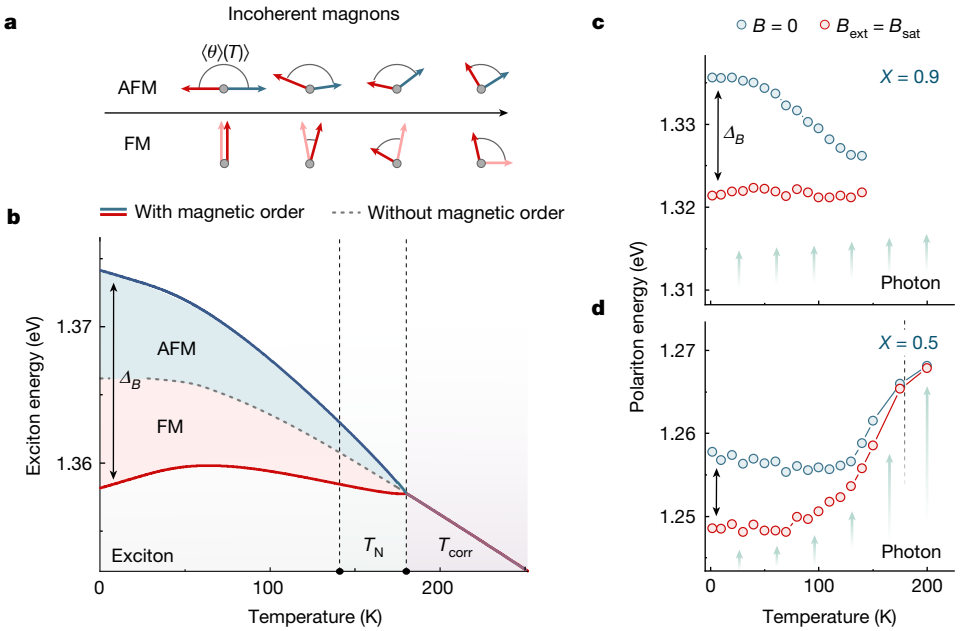

Fig. 4 | Magneto-optical response of CrSBr to incoherent magnons. **a**, At finite temperatures T, incoherent magnons cause spins to fluctuate around their equilibrium position, changing the average angle $\langle\theta(T)\rangle$ between sublattice magnetizations in AFM ($\langle\theta(T)\rangle < \theta(0)$) and FM ($\langle\theta(T)\rangle > \theta(0)$) configurations. FM order is illustrated for $B_{ext} \| c$. **b**, Model of the temperature dependence of excitons in CrSBr for initial AFM and FM order. Effects of the magnetic order strongly impact exciton energies up to a temperature $T_{corr} > T_N$. Here, T_{corr} denotes the temperature up to which magnetic field correlations are observed. **c**,**d**, Temperature-dependent emission energy of polariton branches ($X = 0.9$ (**c**) and $X = 0.5$ (**d**)) measured for initial AFM ($B_{ext} = 0$) and FM ($B_{ext} \| c = B_{sat}$) configuration. The polarization was analysed along the b axis. Due to thermal broadening effects, exciton-like polaritons fade more rapidly from the spectrum. Large photon contributions can overcome the magnon- and phonon-induced shifts of excitons towards lower energies, facilitating a reversal of the temperature-dependent shift.

studies demonstrate time-dependent oscillations of the exciton energy that arise from the periodic modulation of $\theta(t)$ by coherent magnons (compare illustration in Fig. 3a)[24,25]. We observe similar effects for polaritons when we pump a thin crystal enclosed by external mirrors using ultrashort optical pulses and integrate the transient reflectance of resonantly tuned probe pulses in energy. Subsequent to the ultrashort excitation, the polariton reflectance is strongly modulated, as shown in Fig. 3b, by oscillations that excellently match the frequency-field dependence of coherent magnons in CrSBr (compare refs. 24–26 and Supplementary Fig. 13). To highlight the differences between the magneto-optic responses of excitons and polaritons, Fig. 3c–e compares the calculated changes in the reflectance spectrum induced by coherent magnons. Like in the response to a static field, polaritons substantially increase the spectral bandwidth of this magneto-optic effect in CrSBr. Moreover, external cavity mirrors may significantly enhance the sensitivity of optical magnon detection since the small polariton line width causes large relative changes in reflectance.

Beyond this magneto-optical response of CrSBr to coherent magnons, our study unveils a previously unobserved magneto-optic effect that does not require coherence. Magnons excited by non-zero temperatures completely lack the coherence imprinted by ultrafast optical excitation but still change the average angle $\langle\theta(T)\rangle$ (compare Fig. 4a), which in turn affects the exciton component of our polaritons due to the coupling of the electronic and magnetic structures. Analytic magnon theory presented in Supplementary Information Section 3 suggests that below T_N, the temperature dependence of excitons in CrSBr is primarily determined by the population of incoherent magnons. Depending on whether the magnetic structure is initialized with AFM or FM order, incoherent magnons are expected to cause a shift that is linear at low temperatures ($T \ll T_N$) and either decreases or increases the energy of excitons. Because short-range correlations survive longer than the global magnetic ordering[27,28], the general effect extends even beyond the Néel temperature. In CrSBr, the coupling of excitons to magnons thus adds to the typical phonon-related temperature dependence of the exciton energy known from conventional semiconductors[29]. Figure 4b shows the result of our exciton model that includes the effects of the magnetic order and the interaction of excitons with phonons, as described in Supplementary Information Section 4.

The qualitative agreement between this model and the measured temperature–field dependence of an exciton-like polariton branch with $X = 0.9$ shown in Fig. 4c directly confirms our prediction of a magneto-optical response to incoherent magnons. Hence, exciton–polariton spectroscopy emerges as a novel optical probe to monitor the incoherent magnon population and temperature.

The hybridization with photons has a major effect on the thermal response of excitons. For $X = 0.5$, in Fig. 4d, we observe a reversal of the polariton temperature dependence, resulting in a shift towards higher energies. As the field-induced shift Δ_B vanishes in more photon-like polariton branches, effects of magnons and phonons on excitons are increasingly compensated by temperature-induced changes in the static refractive index that determine the energy of the photon component in mesoscopic CrSBr crystals. Overall, our ability to predict this unique magneto-optical response (Supplementary Information Section 4 and Supplementary Figs. 14–16), the impact of external fields and the effects of magnons by numerical models highlight the deterministic nature of engineering magneto-optical properties via strong exciton–photon coupling.

Summary

In conclusion, it is shown that strong exciton–photon coupling can determine the magneto-optical properties of mesoscopic vdW magnetic crystals. Hybrid light–matter excitations in the magnetic semiconductor CrSBr substantially increase the spectral bandwidth of magneto-optic responses by extending correlations between magnetic, electronic and optical properties to states that lie deep within

the band gap of the material. The major role of hybridization in the coupling of magnetism and light evidenced in our study encourages further research to pursue the modification of quantum materials by strong light–matter coupling.

Online content

Any methods, additional references, Nature Portfolio reporting summaries, source data, extended data, supplementary information, acknowledgements, peer review information; details of author contributions and competing interests; and statements of data and code availability are available at https://doi.org/10.1038/s41586-023-06275-2.

1. Garcia-Vidal, F. J., Ciuti, C. & Ebbesen, T. W. Manipulating matter by strong coupling to vacuum fields. *Science* **373**, eabd0336 (2021).
2. Schlawin, F., Kennes, D. M. & Sentef, M. A. Cavity quantum materials. *Appl. Phys. Rev.* **9**, 011312 (2022).
3. Bloch, J., Cavalleri, A., Galitski, V., Hafezi, M. & Rubio, A. Strongly correlated electron–photon systems. *Nature* **606**, 41–48 (2022).
4. Sentef, M. A., Ruggenthaler, M. & Rubio, A. Cavity quantum-electrodynamical polaritonically enhanced electron-phonon coupling and its influence on superconductivity. *Sci. Adv.* **4**, eaau6969 (2018).
5. Ashida, Y. et al. Quantum electrodynamic control of matter: cavity-enhanced ferroelectric phase transition. *Phys. Rev. X* **10**, 041027 (2020).
6. Appugliese, F. et al. Breakdown of topological protection by cavity vacuum fields in the integer quantum hall effect. *Science* **375**, 1030–1034 (2022).
7. Seyler, K. L. et al. Ligand-field helical luminescence in a 2D ferromagnetic insulator. *Nat. Phys.* **14**, 277–281 (2018).
8. Zhang, Z. et al. Direct photoluminescence probing of ferromagnetism in monolayer two-dimensional $CrBr_3$. *Nano Lett.* **19**, 3138–3142 (2019).
9. Kang, S. et al. Coherent many-body exciton in van der Waals antiferromagnet $NiPS_3$. *Nature* **583**, 785–789 (2020).
10. Wilson, N. P. et al. Interlayer electronic coupling on demand in a 2D magnetic semiconductor. *Nat. Mater.* **20**, 1675–1662 (2021).
11. Klein, J. et al. The bulk van der Waals layered magnet CrSBr is a quasi-1D quantum material. *ACS Nano* **17**, 5316–5328 (2023).
12. Huang, B. et al. Layer-dependent ferromagnetism in a van der Waals crystal down to the monolayer limit. *Nature* **546**, 270–273 (2017).
13. Wu, M., Li, Z., Cao, T. & Louie, S. G. Physical origin of giant excitonic and magneto-optical responses in two-dimensional ferromagnetic insulators. *Nat. Commun.* **10**, 2371 (2019).
14. Hwangbo, K. et al. Highly anisotropic excitons and multiple phonon bound states in a van der Waals antiferromagnetic insulator. *Nat. Nanotechnol.* **16**, 655–660 (2021).
15. Dirnberger, F. et al. Spin-correlated exciton–polaritons in a van der Waals magnet. *Nat. Nanotechnol.* **17**, 1060–1064 (2022).
16. Canales, A., Baranov, D. G., Antosiewicz, T. J. & Shegai, T. Abundance of cavity-free polaritonic states in resonant materials and nanostructures. *J. Chem. Phys.* **154**, 024701 (2021).
17. Klingshirn, C. F. *Semiconductor Optics* (Springer, 2012).
18. Munkhbat, B. et al. Self-hybridized exciton-polaritons in multilayers of transition metal dichalcogenides for efficient light absorption. *ACS Photon.* **6**, 139–147 (2018).
19. Fieramosca, A. et al. Tunable out-of-plane excitons in 2D single-crystal perovskites. *ACS Photon.* **5**, 4179–4185 (2018).
20. Dang, N. H. M. et al. Tailoring dispersion of room-temperature exciton-polaritons with perovskite-based subwavelength metasurfaces. *Nano Lett.* **20**, 2113–2119 (2020).
21. Klein, J. et al. Sensing the local magnetic environment through optically active defects in a layered magnetic semiconductor. *ACS Nano* **17**, 288–299 (2023).
22. Lim, H.-T., Togan, E., Kroner, M., Miguel-Sanchez, J. & Imamoğlu, A. Electrically tunable artificial gauge potential for polaritons. *Nat. Commun.* **8**, 14540 (2017).
23. Bajoni, D. et al. Polariton light-emitting diode in a gaas-based microcavity. *Phys. Rev. B* **77**, 113303 (2008).
24. Bae, Y. J. et al. Exciton-coupled coherent magnons in a 2D semiconductor. *Nature* **609**, 282–286 (2022).
25. Diederich, G. M. et al. Tunable interaction between excitons and hybridized magnons in a layered semiconductor. *Nat. Nanotechnol.* **18**, 23–28 (2023).
26. Cham, T. M. J. et al. Anisotropic gigahertz antiferromagnetic resonances of the easy-axis van der Waals antiferromagnet CrSBr. *Nano Lett.* **22**, 6716–6723 (2022).
27. López-Paz, S. A. et al. Dynamic magnetic crossover at the origin of the hidden-order in van der Waals antiferromagnet CrSBr. *Nat. Commun.* **13**, 4745 (2022).
28. Liu, W. et al. A three-stage magnetic phase transition revealed in ultrahigh-quality van der Waals bulk magnet CrSBr. *ACS Nano* **16**, 15917–15926 (2022).
29. O'Donnell, K. & Chen, X. Temperature dependence of semiconductor band gaps. *Appl. Phys. Lett.* **58**, 2924–2926 (1991).

Methods

Crystal growth

CrSBr bulk single crystals were synthesized by a chemical vapour transport method. Chromium (99.99%, −60 mesh; Chemsavers), sulfur (99.9999%, 1-mm to 6-mm granules; Wuhan XinRong New Materials) and bromine (99.9999%; Merck) with a general stoichiometry of about 1:1:1 were placed in a quartz glass ampoule. In fact, sulfur and bromine were used with two atomic percentage excess over the stoichiometry. The ampule (250 × 50 mm) was purged with argon and sealed under high vacuum while the charge was cooled with liquid nitrogen to avoid losses of bromine. The charge was first prereacted at 500 °C, 600 °C and 700 °C for 10 h at each temperature, while the top of the ampule was kept at 100 °C. Finally, the crystal growth was performed in a two-zone gradient furnace, where the charge temperature was gradually increased from 900 °C to 920 °C over a period of 6 days and the temperature of the growth zone was decreased from 900 °C to 800 °C. These temperatures of 920 °C and 800 °C were maintained for another 6 days. Then, the ampule was cooled to room temperature and opened under argon atmosphere in a glove box.

Microcavity fabrication

To fabricate bottom mirrors for our microcavities, highly reflective Bragg mirrors were grown by the plasma-enhanced chemical vapour deposition of eight pairs of silicon nitride–silicon dioxide layers on silicon wafers. First, millimetre-sized CrSBr crystals were thinned down in multiple cycles of stick and release on blue tape (PVC tape 224PR; Nitto) before being transferred onto a polydimethylsiloxane (AD series; Gel-Pak) film. By moderately pressing the polydimethylsiloxane film onto a Bragg mirror (or a SiO_2/Si substrate, oxide thickness of 285 nm) and swiftly releasing it, a multitude of crystals with typical thicknesses of tens to hundreds of nanometres were transferred. Then, a 35-nm-thick layer of gold (or a highly reflective Bragg mirror) was deposited by electron-beam physical vapour deposition (or plasma-enhanced chemical vapour deposition) to form a top mirror.

Optical spectroscopy

For time-integrated spectroscopy measurements, samples were mounted inside a closed-cycle cryostat (attoDRY 2100) with a base temperature of 1.6 K equipped with a 9-T solenoid magnet. Samples can be mounted vertically or horizontally to apply magnetic fields along in-plane or out-of-plane directions. In all configurations, light is focused onto the sample at normal incidence.

Reflectance spectra were obtained by focusing the attenuated output of a spectrally broadband tungsten–halogen lamp to a spot size of 2.0 μm by a ×100 microscope objective (numerical aperture 0.81) mounted inside the cryostat. For polarization-resolved measurements, the reflected signal was analysed by a combination of a half wave plate and a linear polarizer along the axis of maximum PL intensity. Angle-integrated and angle-resolved measurements were recorded by, respectively, focusing either real-space images or the back-focal plane of the objective onto a spectrometer (Princeton Instruments HRS-500) connected to a charge-coupled device. For the PL experiments, unless specified otherwise, a continuous-wave laser with 2.33-eV energy and variable average output power was focused onto the sample to a spot size of 1.0 μm by the same objective used for reflectance spectroscopy. The collected PL signal was directed towards the spectrometer and spectrally filtered to remove the laser emission, and if required, it was analysed by the polarization optics.

Transient optical reflectivity measurements were performed by tuning the output of a titanium sapphire oscillator into resonance with the closely spaced, highly exciton-like branches of an approximately 100-nm-thick CrSBr crystal embedded between two distributed Bragg reflectors. The output was frequency doubled, and the second harmonic and fundamental were separated into pump and probe arms of the experiment by a dichroic mirror. The probe beam was sent to a retroreflector mounted on a motorized translation stage to produce the pump–probe delay. Each beam was sent through a wave plate and polarizer to simultaneously attenuate the beams and align their polarization to the crystal axes. The beams were recombined and sent onto the sample through a microscope objective with a numerical aperture of 0.6. The back-reflected beam was measured on a photodiode with a lock-in amplifier demodulating the signal at the frequency of a mechanical chopper placed in the pump arm of the experiment. To produce the time-domain data, the delay stage was continuously swept at low speed while streaming data from the lock-in amplifier to the host computer at a high sampling rate (more than 100 KHz), which produced time traces with 1-ps resolution in the data presented here. Multiple traces ($4 < N < 25$) were recorded and averaged, depending on the desired signal-to-noise ratio. The samples were kept at 50 K, far below the Néel temperature of approximately 132 K, in an optical cryostat with an integrated vector magnet capable of applying fields along any arbitrary direction on the unit sphere.

Data availability

The main datasets generated and analysed in this study are available at https://doi.org/10.5281/zenodo.7940672 (ref. 30). Supplementary data will be provided by the corresponding authors upon request. Source data are provided with this paper.

30. Dirnberger, F. Magneto-optics in a van der Waals magnet tuned by self-hybridized polaritons. *Zenodo* https://doi.org/10.5281/zenodo.7940672 (2023).

Acknowledgements Work at the City College of New York was supported by the National Science Foundation (DMR-2130544), the National Science Foundation Centers of Research Excellence in Science and Technology - Center for Interface Design and Engineered Assembly of Low-dimensional Systems (CREST IDEALS) centre (V.M.M.), the Defense Advanced Research Projects Agency (DARPA) Nascent Light–Matter Interaction program (R.B.) and the German Research Foundation (451072703; to F.D.). J.Q. and A.A. were supported by the Office of Naval Research, the Air Force Office of Scientific Research and the Simons Foundation. A.A. and V.M.M. acknowledge funding from the US Air Force Office of Scientific Research Multidisciplinary University Research Initiatives (FA9550-22-1-0317). We acknowledge the use of the City University of New York Advanced Science Research Center Nanofabrication Facility for the device fabrication. Z.S. was supported by the European Research Council Czech (ERC-CZ) programme (LL2101) from the Ministry of Education, Youth and Sports. K.M. was supported by the specific university research A2 FCHT 2023 077. The transient magneto-optical measurement at the University of Washington is mainly supported by the Department of Energy, Basic Energy Sciences, Materials Sciences and Engineering Division (DE-SC0012509). This research was supported by an appointment to the Intelligence Community Postdoctoral Research Fellowship Program at the University of Washington, administered by Oak Ridge Institute for Science and Education through an interagency agreement between the US Department of Energy and the Office of the Director of National Intelligence. M.F. and J.K. acknowledge support from the Alexander von Humboldt Foundation. A.K. and F.J.G.-V. acknowledge support from the Spanish Ministry for Science and Innovation–Agencia Estatal de Investigación (PID2021-125894NB-I00 and CEX2018-000805-M through the María de Maeztu program for Units of Excellence in R&D), the Autonomous Community of Madrid, the Spanish Government and the European Union (Mecanismo de Recuperación y Resiliencia (MRR) Advanced Materials MAD2D-CM).

Author contributions F.D. and V.M.M. conceived the experimental idea and interpreted the results together with all of the authors. F.D., J.Q., R.B. and G.M.D. performed the experiments and conducted the data analysis. K.M. and Z.S. synthesized the CrSBr crystals. M.F., A.K. and F.J.G.-V. developed the analytic and numeric theories. F.D. wrote the manuscript with input from all authors and supervised the project with A.A. and V.M.M.

Competing interests The authors declare no competing interests.

Additional information

Supplementary information The online version contains supplementary material available at https://doi.org/10.1038/s41586-023-06275-2.

Correspondence and requests for materials should be addressed to Florian Dirnberger, Andrea Alù or Vinod M. Menon.

Peer review information *Nature* thanks Jae-Ung Lee and the other, anonymous, reviewer(s) for their contribution to the peer review of this work.